Cell Reports

Report

KIF5B plays important roles in dendritic spine plasticity and dendritic localization of PSD95 and FMRP in the mouse cortex *in vivo*

Graphical abstract

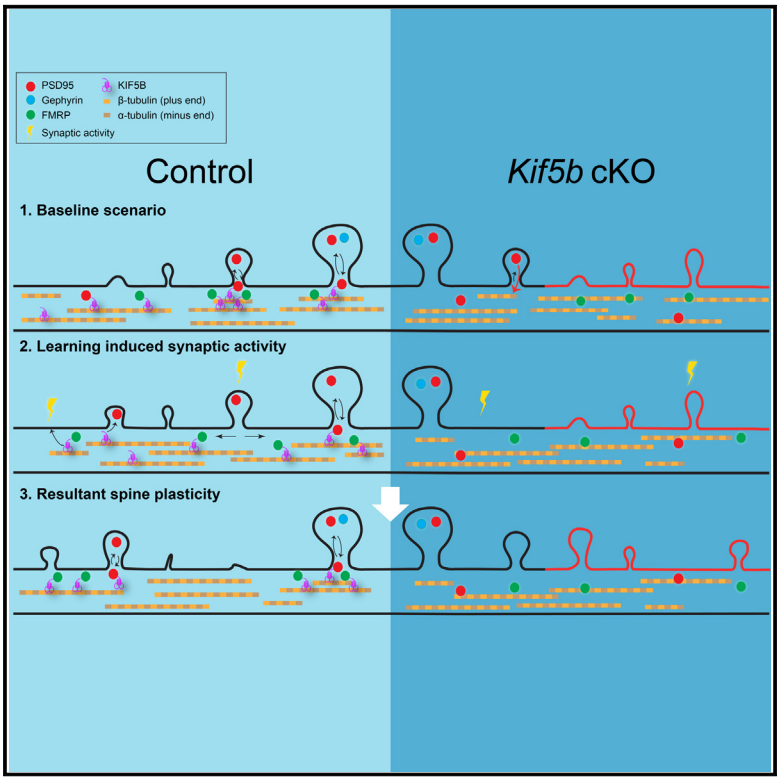

Highlights

- KIF5B regulates synaptic protein composition and turnover of dendritic spines
- KIF5B promotes PSD95 gain and maintenance in dendritic spines
- KIF5B regulates spine-plasticity-related FMRP localization in baseline condition
- KIF5B cKO impairs spine-plasticity-related FMRP localization in fear learning

Authors

Albert Hiu Ka Fok, Yuhua Huang, Beth Wing Lam So, ..., Jiandong Huang, Kwok-On Lai, Cora Sau Wan Lai

Correspondence

kwokolai@cityu.edu.hk (K.-O.L.), coraswl@hku.hk (C.S.W.L.)

In brief

Fok et al. perform intravital imaging to track the translocation of synaptic proteins (PSD95 and gephyrin) and FMRP in dendrites in the mouse frontal cortex. KIF5B is discovered to be necessary for proper PSD95 and FMRP localization in dendrites and activity-dependent dendritic spine plasticity in both baseline and fear learning conditions.

Fok et al., 2024, Cell Reports *43*, 113906
March 26, 2024
https://doi.org/10.1016/j.celrep.2024.113906

CellPress

Cell Reports

CellPress
OPEN ACCESS

Report

KIF5B plays important roles in dendritic spine plasticity and dendritic localization of PSD95 and FMRP in the mouse cortex *in vivo*

Albert Hiu Ka Fok,[1,10] Yuhua Huang,[1,2,10] Beth Wing Lam So,[1] Qiyu Zheng,[1] Chun Sing Carlos Tse,[1] Xiaoyang Li,[1] Kenneth Kin-Yip Wong,[2,3] Jiandong Huang,[1,4,5,6,7] Kwok-On Lai,[8,9,*] and Cora Sau Wan Lai[1,7,11,*]

[1]School of Biomedical Sciences, The University of Hong Kong, Hong Kong SAR, China
[2]Advanced Biomedical Instrumentation Centre, Hong Kong Science Park, Shatin, New Territories, Hong Kong SAR, China
[3]Department of Electrical and Electronic Engineering, The University of Hong Kong, Hong Kong SAR, China
[4]Chinese Academy of Sciences (CAS) Key Laboratory of Quantitative Engineering Biology, Shenzhen Institute of Synthetic Biology, Shenzhen Institutes of Advanced Technology, Chinese Academy of Sciences, Shenzhen, China
[5]Clinical Oncology Center, Shenzhen Key Laboratory for Cancer Metastasis and Personalized Therapy, The University of Hong Kong-Shenzhen Hospital, Shenzhen, China
[6]Guangdong-Hong Kong Joint Laboratory for RNA Medicine, Sun Yat-Sen University, Guangzhou, China
[7]State Key Laboratory of Cognitive and Brain Research, The University of Hong Kong, Hong Kong SAR, China
[8]Department of Neuroscience, City University of Hong Kong, Hong Kong SAR, China
[9]Hong Kong Institute for Advanced Study, City University of Hong Kong, Hong Kong SAR, China
[10]These authors contributed equally
[11]Lead contact
*Correspondence: kwokolai@cityu.edu.hk (K.-O.L.), coraswl@hku.hk (C.S.W.L.)
https://doi.org/10.1016/j.celrep.2024.113906

SUMMARY

Kinesin 1 (KIF5) is one major type of motor protein in neurons, but its members' function in the intact brain remains less studied. Using *in vivo* two-photon imaging, we find that conditional knockout of *Kif5b* (KIF5B cKO) in CaMKIIα-Cre-expressing neurons shows heightened turnover and lower stability of dendritic spines in layer 2/3 pyramidal neurons with reduced spine postsynaptic density protein 95 acquisition in the mouse cortex. Furthermore, the RNA-binding protein fragile X mental retardation protein (FMRP) is translocated to the proximity of newly formed spines several hours before the spine formation events *in vivo* in control mice, but this preceding transport of FMRP is abolished in KIF5B cKO mice. We further find that FMRP is localized closer to newly formed spines after fear extinction, but this learning-dependent localization is disrupted in KIF5B cKO mice. Our findings provide the crucial *in vivo* evidence that KIF5B is involved in the dendritic targeting of synaptic proteins that underlies dendritic spine plasticity.

INTRODUCTION

Kinesin-1 (KIF5, with three members: KIF5A–KIF5C) is one of the kinesin motor families expressed in neurons,[1] which carry dendritic cargoes such as postsynaptic density protein 95 (PSD95), gephyrin (Gep), and fragile X mental retardation protein (FMRP) that are involved in synaptic function and plasticity.[2–9] KIF5B and the closely related KIF5A have distinct functions in dendritic spine formation and transport of RNA-binding protein in cultured hippocampal neurons.[10] Mice with conditional knockout (cKO) of the *Kif5b* gene in the nervous system display deficits in locomotion[11] and learning/memory,[10] indicating non-redundant roles *in vivo*. Our previous study on mice with *Kif5b* cKO in CaMKIIα-expressing neurons (*CaMKIIa*-Cre; *kif5b*$^{fl/fl}$, KIF5B cKO) revealed elevated spine turnover in layer (L) 5 pyramidal neurons.[10] Yet, how KIF5B deficiency affects spine plasticity and the underlying dendritic transport in the intact brain remains elusive.

RESULTS

cKO of *Kif5b* increases dendritic spine turnover and instability in L2/3 pyramidal neurons

We previously found that KIF5B cKO mice exhibited higher spine instability in L5 pyramidal neurons in the frontal association cortex (FrA), which has been implicated in fear learning.[10,12,13] Then, we asked whether KIF5B cKO has the same effect on L2/3, which is known to be upstream of L5 in the FrA local microcircuit.[14,15] Mouse embryos were electroporated *in utero* with constructs that express EYFP, PSD95-mCherry, and Teal-Gep to label spines and synaptic proteins and were subjected to two-photon imaging from postnatal day 38 ± 1 (Figures 1A–1D and S1).[5,16] Compared to control, KIF5B cKO mice showed significant increases in spine formation and elimination rates (Figure 1E), a higher proportion of highly recurrent spines, and lower survival rates of both newly formed and re-formed spines (Figures 1F–1H). The percentage of stable spines that persisted

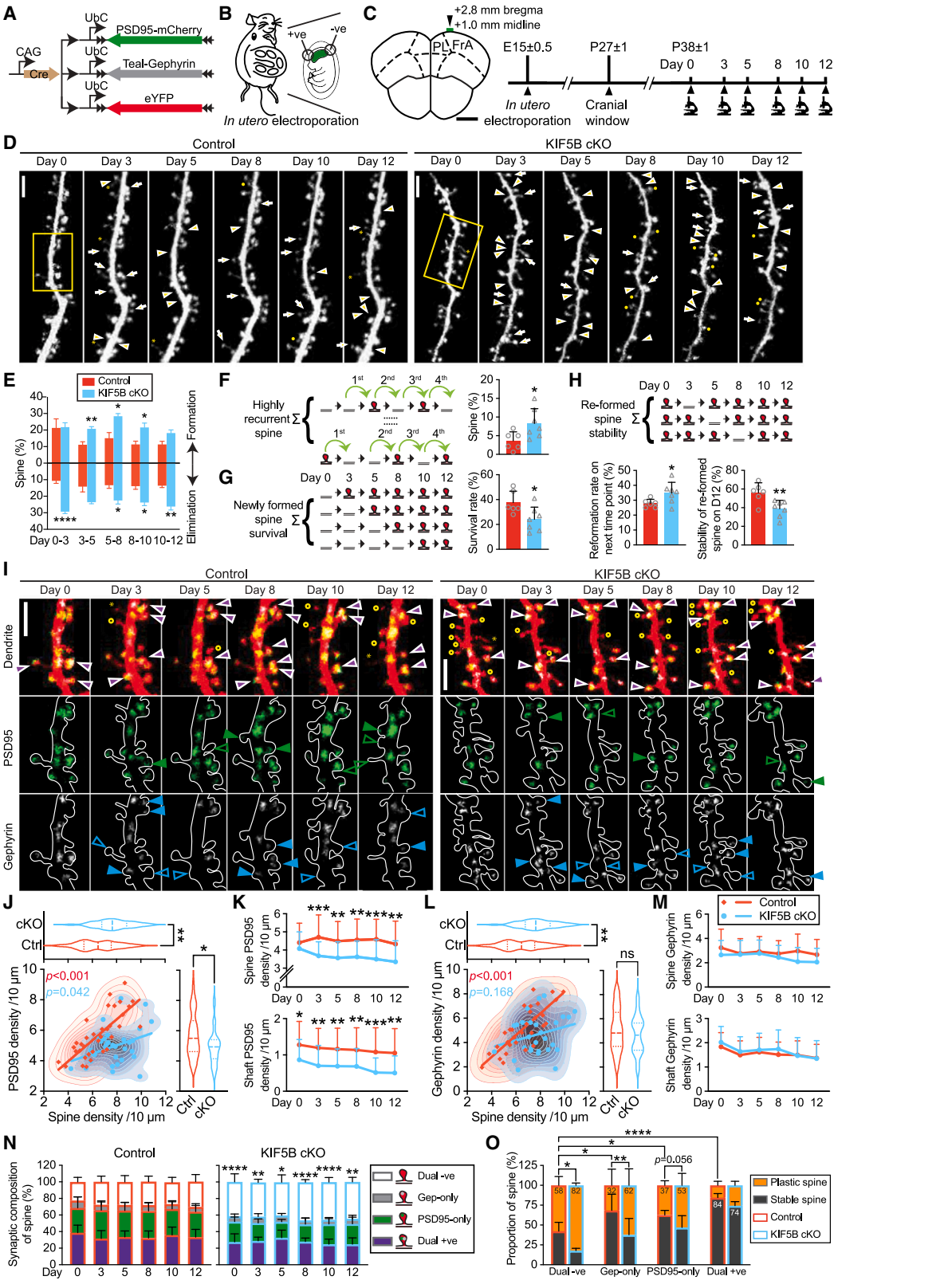

(legend on next page)

until day 12 was also significantly lower in KIF5B cKO mice (Figure S2A). Similar results were found in post-synaptic deletion of *Kif5b* (ps-KIF5B KO), which was done by electroporating the FrA of *Kif5b*$^{fl/fl}$ embryos with a Cre-expressing construct and a Cre-dependent GFP construct (Figures S2B–S2H). To rule out the possibility that our electroporation paradigm might lead to unintended Cre-induced KIF5B KO in GFP-negative axons in the vicinity, we electroporated the same plasmid mixture in Cre-dependent tdTomato reporter mice (Ai9). We confirmed the predominant co-expression of tdTomato and GFP, and even a few GFP-only neurons, without obvious tdTomato-*en passant* axonal boutons in the vicinity of GFP-positive dendrites (Figure S2B). Thus, our approach allowed the study of GFP-positive ps-KIF5B KO neurons receiving normal pre-synaptic inputs. As ps-KIF5B KO could recapitulate the effect of KIF5B cKO in L2/3 pyramidal neurons, our data suggest that KIF5B has a specific function in the post-synaptic regulation of spine plasticity beyond axonal transport.

Lower stability of the dendritic spine is associated with fewer PSD95 puncta in the dendritic spine in KIF5B cKO mice

We next examined spine plasticity together with the dynamics of excitatory and inhibitory synaptic scaffolding proteins (Figures 1I and S2I–S2K). KIF5B cKO mice showed a higher spine density but lower density of PSD95 puncta on day 0 (Figures 1J and 1K). However, KIF5B cKO did not alter the density of Gep puncta (Figures 1L and 1M). We found that the total density of PSD95 and Gep puncta was significantly correlated with spine density in control (Figures 1J and L), but this correlation between Gep and spine density was not observed in KIF5B cKO mice (Figure 1L), suggesting that the lack of KIF5B affects the normal relationship between synaptic protein distribution and spine density. Next, we categorized the synaptic composition of spines into four types: dual positive (+ve), dual negative (−ve), PSD95-only, and Gep-only spines. KIF5B cKO mice had fewer PSD95-only and more dual −ve spines compared to control (Figures 1N and S2K). The stability of dual −ve spines was significantly lowered in KIF5B cKO mice than control (Figure 1O). Taken together, KIF5B cKO decreased the proportion of PSD95-positive spines and increased dual −ve spines. Notably, KIF5B cKO also significantly reduced the stability of Gep-only spine (Figure 1O), indicating that its impact on spine stability may involve various mechanisms. Since Gep-only spines only make up of a small proportion of spines (Figure 1N), our data suggest that the deficit in PSD95 acquisition in spines accounts for the main cause of the overall spine instability in KIF5B cKO mice.

cKO of *Kif5b* reduces PSD95 puncta gain and maintenance in dendritic spines, leading to more spine elimination

PSD95 and Gep puncta are constantly gained and lost in spines.[16–20] We next investigate if the stabilities of PSD95 and Gep puncta in spines are affected by *Kif5b* deletion (Figure 2A). The PSD95 stability in PSD95-only spines was significantly lower compared to dual +ve spines in KIF5B cKO mice (Figure 2A). KIF5B cKO mice also had significantly fewer PSD95-positive spines compared to control without affecting the Gep-positive spines (Figures 2B and 2C), further suggesting a deficit of PSD95 localization in KIF5B cKO mice instead of Gep localization in spines. Since PSD95 recruitment is associated with higher spine stability,[5,16,20] we next traced the fate of PSD95-negative spines across the whole imaging period in our data. Compared to control, the KIF5B cKO neurons had a lower proportion of PSD95-negative spines gaining PSD95 and a higher proportion of these spines were eliminated (Figures 2D and S3A–S3E). To confirm this, we further separated PSD95 gain into two

Figure 1. KIF5B cKO leads to higher dendritic spine turnover and fewer PSD95 in both dendrites and dendritic spines

(A and B) Plasmid constructs for labeling of dendritic spines (EYFP), excitatory synapses (PSD95-mCherry), and inhibitory synapses (Teal-gephyrin) were expressed in cortical L2/3 pyramidal neurons of the frontal cortex by *in utero* electroporation.

(C) Schematic diagram showing the cranial window implantation on the frontal association cortex (FrA) and the experimental timeline. Scale bar, 1 mm.

(D) Representative images of dendrites of L2/3 pyramidal neurons in the FrA. Arrows denote spine formation, and arrowheads denote spine elimination, compared to day 0. Asterisks denote filopodia. Yellow circles denote recurrence spines. Yellow rectangles indicate the region of interest in (I). Scale bar, 5 μm.

(E) Quantification of the rate of spine formation and elimination between days 0 and 3, 3 and 5, 5 and 8, 8 and 10, and 10 and 12.

(F–H) Schematic diagram and quantification of highly recurrent spines (F), total newly formed spines that persisted until day 12 (G), and re-formed spines at next time point (H, left) and the stability of re-formed spines on day 12 (H, right).

(I) Representative images of dendrites with PSD95-mCherry and Teal-gephyrin. Purple arrowheads denote both PSD95 and gephyrin-positive (dual +ve) spines. Yellow empty circles denote dual negative (dual −ve) spines. Empty arrowheads denote elimination of PSD95 (green) or gephyrin (blue), and filled arrowheads denote formation of PSD95 or gephyrin, compared to the previous time point. Asterisks denote filopodia. Scale bar, 5 μm.

(J) Quantification and correlation of total PSD95 and spine densities on day 0 for control and KIF5B cKO mice. Each data point in the scatterplot represents the PSD95 density and spine density of each dendrite (red: control, $r = 0.7607$, $p < 0.001$; blue: KIF5B cKO, $r = 0.3354$, $p = 0.042$). Dashed lines in violin plots represent the median, and the dotted lines represent the quartiles of spine and PSD95 densities.

(K) Density of PSD95 in dendritic spine and shaft at each imaging time point.

(L) Quantification and correlation of total gephyrin and spine densities on day 0 for control and KIF5B cKO mice. Each data point in the scatterplot represents the gephyrin density and spine density of each dendrite (red: control, $r = 0.8130$, $p < 0.001$; blue: KIF5B cKO, $r = 0.2582$, $p = 0.168$). Dashed lines in violin plots represent the median, and the dotted lines represent the quartiles of spine and gephyrin densities.

(M) Density of gephyrin in dendritic spine and shaft at each imaging time point.

(N) Quantification of spine synaptic composition in control and KIF5B cKO mice at each imaging time point. Statistical test compares proportion of dual −ve spines.

(O) Quantification of stability of different spine types between days 0 and 12. Numbers in bars indicate the mean values. Stable spines are defined as spines that are present on all imaging time points, and the rest are plastic spines. Control: n = 6, KIF5B cKO: n = 7.

Data are presented in mean +SD in (E)–(H), (K), and (M)–(O). *$p < 0.05$, **$p < 0.01$, ***$p < 0.001$, and ****$p < 0.0001$. Two-way ANOVA with post hoc Sidak's test for (E), (K), and (M)–(O). Student's t test for (F)–(H), (J), and (L). Pearson's correlation for (J) and (L).

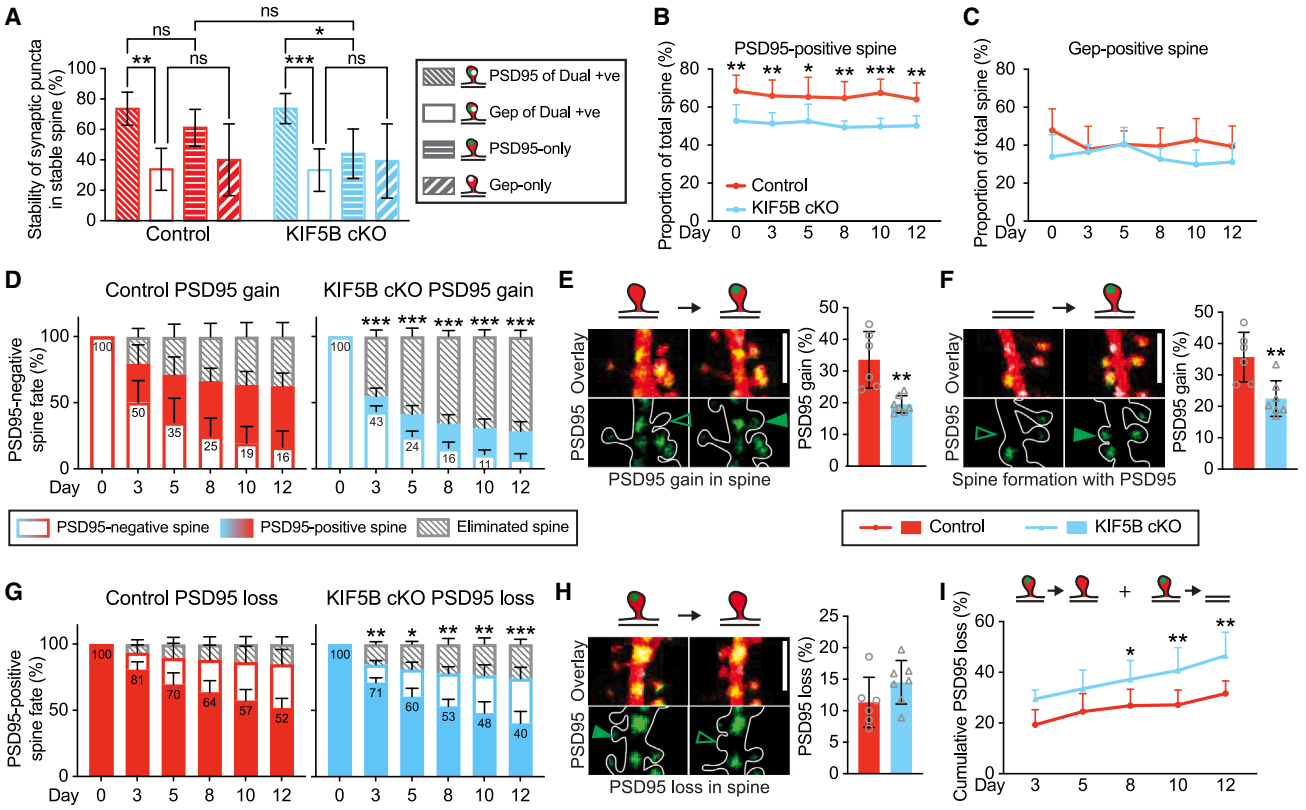

Figure 2. KIF5B cKO reduces PSD95 gain and maintenance in dendritic spines

(A–C) Quantification of the proportion of PSD95 and gephyrin puncta stability on stable spines that persisted until day 12 (A), PSD95-positive spines (B), and gephyrin-positive spines (C) at each imaging time point.

(D) Quantification of the fate of PSD95-negative spines identified on day 0 over 12 days. Statistical test compares proportion of eliminated spines.

(E) Quantification of the proportion of PSD95-negative spines that gained PSD95 at the consecutive time point over 12 days.

(F) Quantification of the proportion of PSD95-positive newly formed spines among all newly formed spines at the consecutive time point over 12 days.

(G) Quantification of the fate of PSD95-positive spines identified on day 0 over 12 days. Statistical test compares proportion of eliminated spines.

(H) Quantification of the loss rate of PSD95 from stable spines at the consecutive time point over 12 days.

(I) Schematic diagram and quantification of the cumulated loss of PSD95 from stable spines and eliminated spines at different time points compared to day 0.

Control: n = 6, KIF5B cKO: n = 7.

Data are presented in mean ± SD for (A), (E), (F), and (H) and +SD for (B)–(D), (G), and (I). Scale bar, 5 μm. *p < 0.05, **p < 0.01, and ***p < 0.001. Two-way ANOVA with post hoc Sidak's test for (A)–(D), (G), and (I). Student's t test for (E), (F), and (H).

categories between two consecutive imaging time points over 12 days regardless of the starting time point of tracking: spine with a gain of PSD95 (Figure 2E) and new spine formation with concurrent PSD95 puncta (Figure 2F). We found that KIF5B cKO reduced PSD95 gain in both categories, indicating that *Kif5b* deletion affects both existing and newly formed spines. In addition, KIF5B cKO mice showed a lower proportion of stable PSD95-positive spines and a higher proportion of eliminated PSD95-positive spines compared to control (Figures 2G and S3F).

Although PSD95 loss from stable spines between all consecutive imaging time points was not significantly different between control and KIF5B cKO mice (Figure 2H), we found a significantly higher cumulative PSD95 loss from stable and eliminated spines in KIF5B cKO mice (Figure 2I). This could reflect a limitation of the temporal resolution of the experiments to capture PSD95 loss prior to spine elimination. We repeated the same analysis for Gep and found that *Kif5b* deletion did not affect Gep gain and loss in spines (Figures S3G–S3J). Therefore, *Kif5b* deletion specifically reduces PSD95 puncta in spines, resulting in more dual −ve spines that are less stable. Taken together, our data suggest that KIF5B regulates spine plasticity by affecting PSD95 availability in spines.

cKO of *Kif5b* dysregulates FMRP localization and dynamics in both dendrites and dendritic spines

FMRP is a known cargo of KIF5s that controls PSD95 translation/degradation and spine morphogenesis.[2,4,6,7,10,21–26] To investigate whether KIF5B also regulates the FMRP dendritic localization and FMRP-associated spine plasticity, L2/3 pyramidal neurons were transfected with constructs to label spines (dsRed) and FMRP (FMRP-GFP) (Figures 3A–3C). We quantified the spine plasticity and FMRP dynamics in basal dendrites since FMRP is more localized in proximal dendrites[27,28] (Figure S4A).

CellPress
OPEN ACCESS

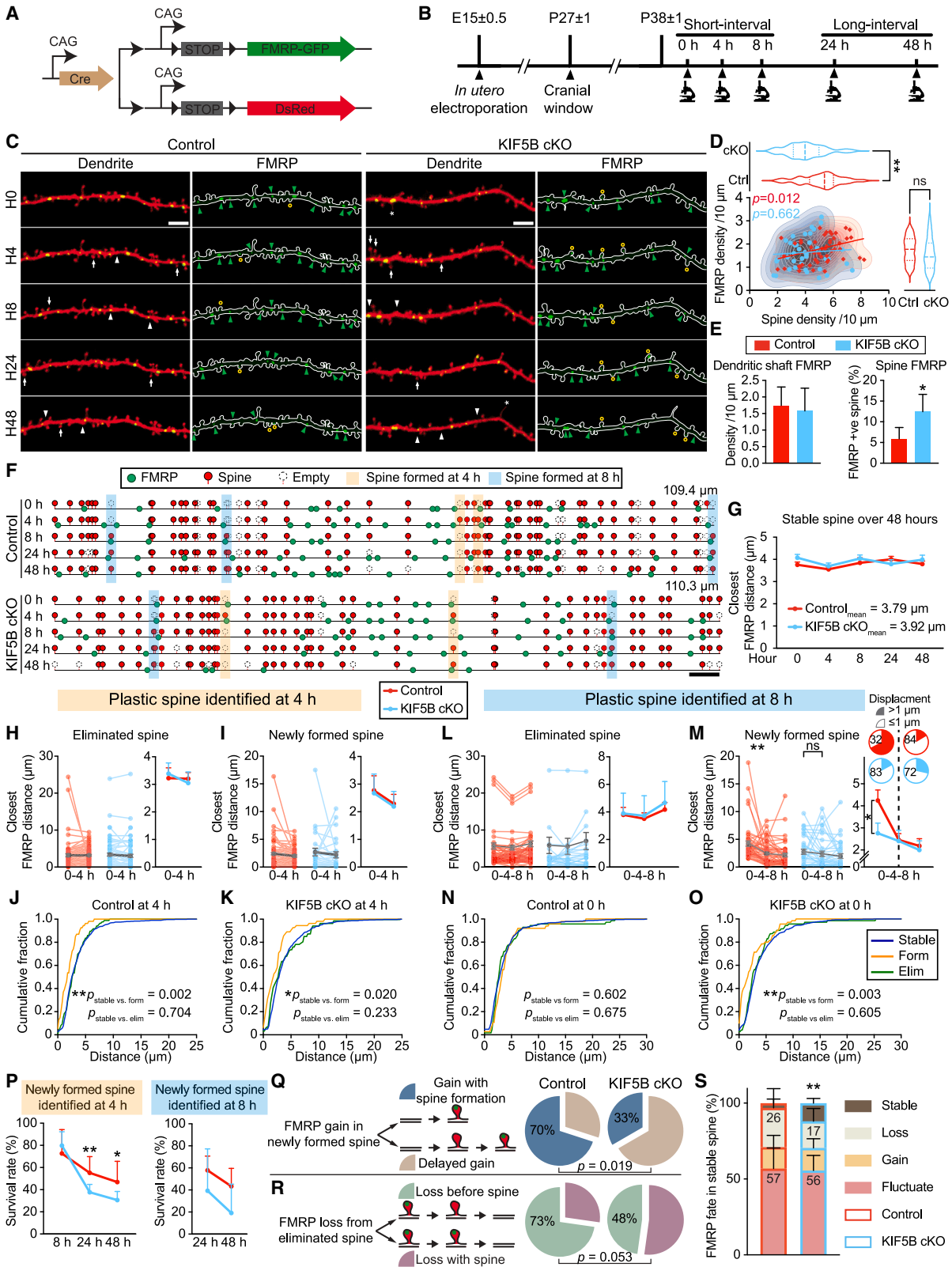

(legend on next page)

There is limited literature that have studied FMRP dendritic localizations *in vivo*, so we first characterized dendritic FMRP puncta distribution in dendrites. KIF5B cKO mice showed a lower spine density, but no significant difference in total FMRP density at 0 h when compared to control (Figures 3D, S4B, and S4C). The majority of the FMRP puncta were localized in dendritic shafts in both control and KIF5B cKO mice (Figure S4D). The total density of FMRP significantly correlated with spine density in control but not in KIF5B cKO mice (Figure 3D). There was also a significantly higher proportion of FMRP-positive spines in KIF5B cKO mice at 0 h (Figure 3E). These data suggest that KIF5B deficiency dysregulates the normal distribution of FMRP in relation to spine density.

Next, we examined if FMRP localization in dendritic shaft associates with spine plasticity. Unlike *in vitro* time-lapse imaging studies,[2,10] we could not observe real-time (in minutes) translocation of FMRP puncta with our *in vivo* approach (data not shown). Therefore, we addressed the association between FMRP and spine plasticity by measuring the relative distance of the closest shaft FMRP puncta to different spine types: stable, eliminated, and newly formed spines in hour intervals (Figure 3F). On average, the closest shaft FMRP distance to stable spines was similar between control and KIF5B cKO mice (Figure 3G). For the spine plastic events that occurred at 4 h, FMRP was found to be localized closer to the sites of spine formation 4 h prior to their formation and remained close at 4 h compared to stable spines in both control and KIF5B cKO mice (Figures 3H–3K). This suggests that FMRP localization is associated with spine formation.

We performed the same analysis for the relative distance between FMRP and plastic spines identified at 8 h. The relative distance between FMRP and eliminated spine at 8 h was similar to that of stable spines for both control and KIF5B cKO mice from 0 to 8 h (Figures 3L, 3N, and 3O). However, the closest FMRP distance to 8 h newly formed spines was 4.24 ± 0.47 μm at 0 h and was shortened over time in control (Figures 3F, highlighted by blue rectangle, and 3M). Also, a lower proportion of FMRP puncta showed more than 1 μm displacement in KIF5B cKO mice compared to control from 0 to 4 h (Figure 3M), indicating lower mobility of FMRP puncta in KIF5B cKO mice. When we compared the relative distance of FMRP at 0 h to the sites of plastic spines identified at 8 h, the newly formed spine was significantly closer than that of stable and eliminated spines in KIF5B cKO mice but not in control (Figures 3N and 3O). This suggests that FMRP localization around plastic spines is likely selectively regulated by KIF5B.

Indeed, we found that the distribution of FMRP puncta in dendrites was not random when compared to random distribution simulation (Figures S5A–S5F). The FMRP pairs within 10 μm were distributed further away from each other than they would be in a random distribution fashion (Figures S5A–S5F). Furthermore, we found that FMRP puncta are distributed closer to spines than FMRP puncta simulated in a randomly distributed manner in both control and KIF5B cKO mice, suggesting that FMRP distribution in dendrites was selectively regulated (Figures S5G–S5L). It is also noted that the reduction of relative distance between dendritic shaft FMRP puncta and newly formed spines

Figure 3. KIF5B cKO dysregulates FMRP localization and dynamics in both dendrites and dendritic spines

(A) Plasmid constructs for labeling of dendritic spines (dsRed) and fragile X mental retardation protein (FMRP-GFP) in cortical L2/3 pyramidal neurons.

(B) Experimental timeline.

(C) Representative images of basal dendrite of L2/3 pyramidal neurons in the FrA with FMRP-GFP puncta. White arrows denote spine formation, and white arrowheads denote spine elimination, compared to 0 h. Asterisks denote filopodia. Green arrowheads denote FMRP puncta in dendrites. Yellow circles denote FMRP puncta in spines. Scale bar, 5 μm.

(D) Quantification and correlation of total FMRP and spine densities at 0 h. Each data point in the scatterplot represents the FMRP density and spine density of each dendrite (red: control, $r = 0.3635$, $p = 0.012$; blue: KIF5B cKO, $r = 0.0733$, $p = 0.662$). Dashed lines in violin plots represent the median, and the dotted lines represent the quartiles of spine and total FMRP densities.

(E) Quantification of the dendritic shaft FMRP density and the proportion of FMRP-positive (+ve) spines at 0 h.

(F) Representative dynamic shaft FMRP-spinogram shows the location of dendritic spines (red) and shaft FMRP puncta (green) in dendrite. Locations of eliminated spines and newly formed spines before formation are presented as empty circle. Examples of newly formed spines identified at 4 (beige rectangle) and 8 h (blue rectangle) are highlighted. Scale, 5 μm.

(G) Quantification of the closest shaft FMRP puncta relative distance from stable spines at each imaging time point.

(H and I) Quantification of the closest shaft FMRP puncta relative distance at 0 and 4 h time points from plastic spines identified at 4 h: eliminated spines (H) and newly formed spines (I). Every data point on the left (red: Control; blue: KIF5B cKO) represents the distance between a plastic spine identified at 4 h and its closest FMRP punctum at the respective time point.

(J and K) Distribution of the closest shaft FMRP puncta at 4 h from stable (blue line), newly formed (orange line), and eliminated (green line) spines identified at 4 h. FMRP puncta are relatively closer to newly formed spines in both control (J) and KIF5B cKO (K).

(L and M) Quantification of the closest shaft FMRP puncta relative distance at 0, 4, and 8 h from plastic spines identified at 8 h: eliminated spines (L) and newly formed spines (M). Every data point on the left (red: control; blue: KIF5B cKO) represents the distance between a plastic spine identified at 8 h and its closest FMRP punctum at the respective time point. The pie charts in (M) indicate the proportion of FMRP puncta displacement degree in 0–4 and 4–8 h (numbers indicate the mean value). Displacement >1 μm (solid) and ≤1 μm (empty).

(N and O) Distribution of the closest shaft FMRP puncta at 0 h from stable (blue line), newly formed (orange line), and eliminated (green line) spines identified at 8 h in control (N) and KIF5B cKO (O).

(P) Survival rate of the newly formed spines identified at 4 (left) and 8 h (right) at each subsequent time point.

(Q and R) Schematic and proportion of FMRP puncta found in spines at the same time point of spine formation (blue: gain with spine formation) or later time point (beige: delayed gain) in 0–8 h (Q) and lost from spines before spine elimination (green: loss before spine) or same time point (purple: loss with spine) in 0–8 h (R).

(S) Quantification of the fate of FMRP puncta in stable spines that persisted from 0 until 8 h. Statistical test compares proportion of stable FMRP puncta. Control: n = 6, KIF5B cKO: n = 5.

Data are presented in mean +SD for (E), (P), and (S) and +SEM for (G)–(I), (L), and (M). Scale bar, 5 μm. *$p < 0.05$ and **$p < 0.01$. Two-way ANOVA with post hoc Sidak's test for (G)–(I), (L), (M), and (P). Student's t test for (D), (E), and (S). Pearson's correlation for (D). Chi-squared test for (Q) and (R). Kolmogorov-Smirnov test for (J), (K), (N), and (O).

might be a transient event (within 8 h), as we did not observe similar changes in newly formed spines that were identified at 24 and 48 h (Figures S4E–S4H). The survival rate of newly formed spines identified at 4 h was also significantly lower at 24 and 48 h in KIF5B cKO mice (Figure 3P). These data suggest that the newly formed spines in KIF5B cKO mice may arise based on mislocalized FMRP, which is not aligned with bona fide presynaptic cues and proper postsynaptic protein transport mechanisms necessary for stable spine formations, hence a lower rate of survival. Taken together, the FMRP puncta on dendritic shaft were localized near newly formed spines within an 8 h period before spine formation in control mice, and this preceding translocation was abolished in KIF5B cKO mice.

Next, we examined the dynamics of FMRP puncta in spines. During the 8 h imaging period, most of the FMRP puncta in newly formed spines were found concurrently with the spine formation in the control, while most of the new spines in KIF5B cKO mice showed a delayed gain of FMRP (Figure 3Q). For elimination of FMRP +ve spines, the majority of FMRP puncta were lost from the spine head before the spine elimination in control, but not in KIF5B cKO mice (Figure 3R). We next investigated the dynamics of FMRP (fluctuate, gain, loss, and stable) in stable spines that persisted over 8 h. More than half of the FMRP puncta fluctuated in spines in both the control and KIF5B cKO mice, consistent with previous studies showing activity-dependent FMRP trafficking and translation around synapses *in vitro* (Figure 3S).[28–32] However, there was less FMRP puncta loss and significantly more stable FMRP puncta in spines in KIF5B cKO mice (Figure 3S). Since FMRP also regulates synaptic plasticity as a repressor of translation,[33] the abnormally low FMRP puncta turnover rate in spines may suppress proper local protein synthesis and lead to aberrant synaptic function and plasticity in KIF5B cKO mice. Our findings therefore suggest that KIF5B plays specific roles in spine plasticity through regulating the localization and dynamics of FMRP.

cKO of *kif5b* impairs fear-learning-dependent spine plasticity and the associated FMRP localization

Previous study showed that fear conditioning (FC) leads to spine elimination while fear extinction induces spine formation on the apical dendrites of L5 pyramidal neurons in the FrA.[12] Since we previously found that *Kif5b* deletion impaired fear memory,[10] we next examined spine plasticity and FMRP localization in the basal dendrite of L2/3 pyramidal neurons after fear learning. Head-fixed awake imaging was adopted to minimize the impact of anesthesia (Figures 4A–4C). We found that the KIF5B cKO paired group (conditioned stimulus [CS]-foot shock pairing) showed a significantly lower FC-induced freezing behavior and FC-induced spine elimination when compared to the control paired group; it also had a significant increase of spine formation when compared to the control unpaired group (Figures 4D and 4E). The degree of freezing response in recall was significantly correlated with spine elimination, suggesting that these spine changes were associated with fear learning behavior (Figure S6A). On the other hand, repeated exposure to CS in fear extinction induced a significant increase of spine formation in the control paired group but not in KIF5B cKO group (Figures 4F and 4G). Therefore, deletion of *Kif5b* impaired fear learning and the learning-induced spine plasticity in L2/3 pyramidal neurons.

Next, we asked if FMRP localization is associated with FC- and extinction-induced spine plasticity. We quantified the relative distance between shaft FMRP puncta and the closest eliminated spines or newly formed spines induced by fear learning. In control, FC induced no significant difference in the FMRP relative distance to both eliminated spines or newly formed spines when comparing paired and unpaired control groups (Figures 4H and 4I). For fear extinction, while the rate of spine formation was significantly higher in the control paired group than in the unpaired group, we found that the median FMRP relative distance to newly formed spines was shorter in the control paired group, indicating that more FMRP puncta were localized closer to the newly formed spines, but no such observations can be found between the FMRP relative distance and the sites of spine elimination (Figures 4J and 4K). Therefore, FMRP dendritic localization is associated with spine formation but not spine elimination, which is consistent with our findings in baseline FMRP localization (Figure 3).

Interestingly, *Kif5b* deletion led to abnormal FMRP puncta proximity to plastic spines: (1) after FC, the FMRP puncta population shifted further away from eliminated spines (Figure 4H) but shifted closer to newly formed spines in the KIF5B cKO paired group when compared to the control paired group (Figure 4I), and (2) after fear extinction, the FMRP puncta population shifted closer to eliminated spines and further away from newly formed spines in the KIF5B cKO paired group (Figures 4J and 4K). In summary, there is specific fear-learning-dependent FMRP localization toward newly formed spines but not eliminated spines after fear extinction in control. Notably, *Kif5b* deletion not only abolished fear-learning-induced spine plasticity but also altered this learning-dependent FMRP dendritic localization, underscoring the specific roles of KIF5B in experience-dependent spine plasticity by regulating the FMRP localization.

DISCUSSION

Heightened dendritic spine turnover is commonly observed in various mouse models of neurological and psychiatric diseases with behavioral and learning deficits.[4,18,34–37] Here, we demonstrated that conditional[38–41] and post-synaptic KO of *Kif5b* heightened spine turnover in L2/3 pyramidal neurons. By evaluating two synaptic scaffolding proteins transported by KIF5s,[3,8,42] we found that the increased spine instability in KIF5B cKO mice was related to dendritic localization of PSD95 but not Gep. Although previous studies proposed lateral diffusion as the major mode of PSD95 trafficking to spines,[43–45] a recent study demonstrated that microtubule invasion into spines was a predicative factor for PSD95 enrichment,[46] suggesting potential KIF5-dependent PSD95 trafficking into spines. Bleed through of YFP signals to blue channel (Gep-Teal) was not observed in our images, and the Gep-Teal image was essentially the same before and after conducing spectral linear unmixing (Figure S1). However, it is noted that Gep density in spines in the FrA was higher than the primary visual cortex reported

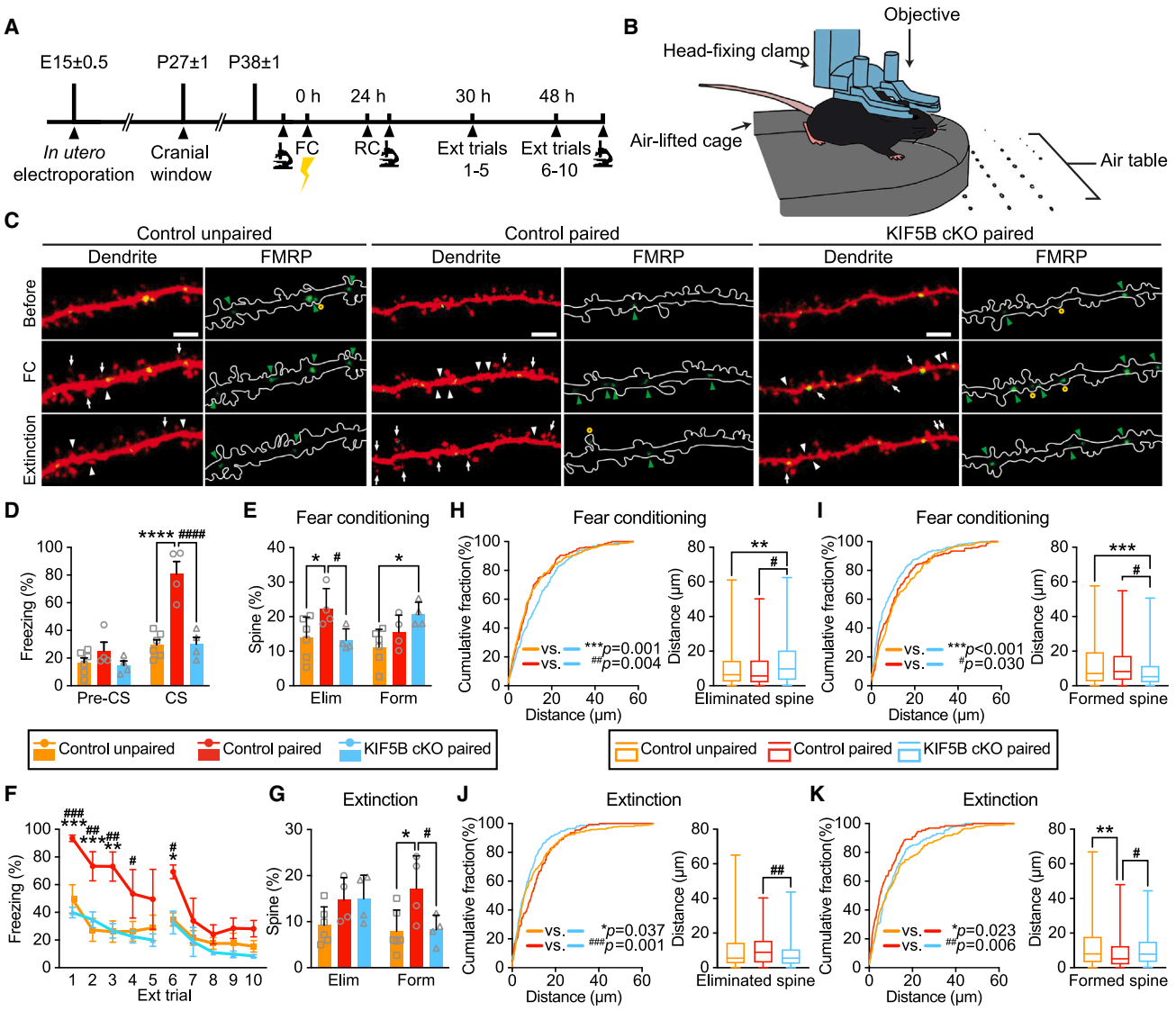

Figure 4. KIF5B cKO impairs fear-learning-dependent spine plasticity and the associated FMRP localization

(A and B) Experimental timeline for fear conditioning (FC), recall test (RC), and extinction (Ext trials) (A) with head-fixed awake animal imaging (B).

(C) Representative images of basal dendrites (dsRed) of L2/3 pyramidal neurons with FMRP-GFP. White arrows denote spine formation, and white arrowheads denote spine elimination, compared to 0 h. Green arrowheads denote FMRP puncta in dendrites. Yellow circles denote FMRP puncta in spines. Scale bar, 5 μm.

(D and F) Quantification of freezing response in RC during pre- and conditioned stimulus (CS) periods (D) and during the CS period of fear extinction (F).

(E and G) Quantification of the rate of spine elimination (Elim) and formation (Form) after FC (E) and after fear extinction (G).

(H and I) Distribution (left) and the box and whisker plots (right) of (H) the closest eliminated spines and (I) the closest newly formed spines distance from shaft FMRP puncta after FC. Solid line in boxplots represent the median relative distance.

(J and K) Distribution (left) and the box and whisker plots (right) of (J) the closest eliminated spines and (K) the closest newly formed spines distance from shaft FMRP puncta after fear extinction. Solid line in boxplots represents the median relative distance. Control paired: n = 6, control unpaired: n = 4, KIF5B cKO: n = 4. Data are presented in mean ± SD for (F) and +SD for (D), (E), and (G). *p < 0.05, **p < 0.01, ***p < 0.001, and ****p < 0.0001 compared to control unpaired. #p < 0.05, ##p < 0.01, ###p < 0.001, and ####p < 0.0001 compared to control paired. Two-way ANOVA with post hoc Tukey's test for (D)–(G). Kruskal-Wallis with post hoc Dunn's test for (H)–(K). Kolmogorov-Smirnov test for (H)–(K) cumulative fraction.

previously,[16] suggesting a different distribution of Gep in FrA compared to other cortical regions.

Besides protein trafficking, local mRNA translation and protein degradation could affect the availability of PSD95 in spines.[22] Indeed, FMRP can regulate PSD95 availability via mRNA translation and proteasomal degradation. Although FMRP is a well-established translational repressor, recent studies have demonstrated the regulation of nearly all aspects of gene expression by FMRP (see review[47]). Different from cultured neurons,[2,10,48,49] our data showed that FMRP puncta appeared to move slower *in vivo* and were translocated closer to the sites of newly formed spines 4–8 h preceding to the spine formation in the control mice.

KIF5B cKO mice lacked such FMRP dendritic translocation, although eventual spine formation still occurred closely around FMRP puncta. We speculate that KIF5B's absence might compromise this activity-dependent dendritic targeting of FMRP for mRNA delivery and local translation and lead to lower survival rate of spines. On the other hand, although the relative distance of FMRP to eliminated spines in KIF5B cKO mice was significantly different when compared to the control paired group after both FC and extinction, there was no significant difference between the unpaired and paired groups in control mice (Figures 4H and 4J). Furthermore, FMRP puncta were localized closer to the newly formed spines than to eliminated spines in the control paired-extinction group (Figure S6B). Therefore, the dendritic localization of FMRP is likely associated with learning-dependent spine formation but not elimination. Our data suggest that KIF5B could play a more intricate role in cargo transport than generally believed: KIF5B fine-tunes the precise positions of FMRP close to individual spines, and its absence could compromise proper synaptic plasticity, in particular spine formation events and spine stability.

Overall, our study demonstrated specific functions of KIF5B in PSD95 and FMRP dendritic localization, as well as spine plasticity both in baseline condition and in fear learning. The stability of PSD95 in spine could be maintained directly by KIF5B-mediated trafficking. KIF5 might also mediate dendritic trafficking of other synaptic proteins, which can be concurrently regulated by FMRP for local translation; these could all contribute to the modification of spine plasticity and maintenance.

Limitations of the study

First, our *in utero* electroporation approach is advantageous in co-expressing multiple fluorescence-tagged target proteins in layer-specific cortical neurons but implies their overexpression. Future experiments can consider using transgenic mice or Cas9/SLENDR to tag endogenous PSD95 or FMRP *in vivo*.[50] Second, based on prior knowledge that FMRP interacts with the 3′ UTR of PSD95 mRNA, it is conceivable that KIF5B also modulates synaptic PSD95 during spine plasticity through translational control via FMRP. However, the PSD95-mCherry plasmids in the study do not contain the 5′ UTR and the 3′ UTR.[16] Therefore, our current findings on the transport of exogenous PSD95-mCherry could not address the causal relationship between FMRP and PSD95 puncta distribution. Third, PSD95 and FMRP were not simultaneously imaged at the same time. Fourth, the temporal resolution of *in vivo* imaging experiments was limited, and the actual movement of individual puncta cannot be tracked over the imaging time course. Finally, the current study is limited to provide interpretation of the KIF5B-FMRP association in auditory-cued FC.

STAR★METHODS

Detailed methods are provided in the online version of this paper and include the following:

- KEY RESOURCES TABLE
- RESOURCE AVAILABILITY
  - Lead contact
  - Materials availability
  - Data and code availability
- EXPERIMENTAL MODEL AND STUDY PARTICIPANT DETAILS
  - Animals
- METHOD DETAILS
  - Auditory-cued fear conditioning and fear extinction
  - DNA constructs
  - In utero electroporation
  - *In vivo* imaging of dendritic spines, synaptic markers and FMRP-GFP
- QUANTIFICATION AND STATISTICAL ANALYSIS
  - Data analysis
  - Statistical analysis

SUPPLEMENTAL INFORMATION

Supplemental information can be found online at https://doi.org/10.1016/j.celrep.2024.113906.

ACKNOWLEDGMENTS

The authors would like to thank the HKU CPOS and CCMR for their technical support. The authors would like to thank Leonard W. Cheung for his support on mouse genotyping and Catherine Ayoub for her help in sketching some experiment schematic illustrations. This work was supported by the Research Grant Council of Hong Kong (17102120, 17108821, and 17103922 to C.S.W.L.; 17106018, 17117720, 11102422, and C1024-22G to K.-O.L.; 17124921 to J.H.; and 17210522, C7074-21G, 17205321, 17200219, and 17209018 to K.K.-Y.W.), the University Grants Committee of Hong Kong (AoE/M-604/16 and T13-605/18-W to K.-O.L.), the National Natural Science Foundation of China (NSFC/RGC/JRF N_HKU735/21 to C.S.W.L.), the Health and Medical Research Fund (HMRF 09200966 to C.S.W.L. and 06172986 to K.-O.L.), and the Health@InnoHK program of the Innovation and Technology Commission of the Hong Kong SAR Government to K.K.-Y.W.

AUTHOR CONTRIBUTIONS

A.H.K.F., Y.H., K.-O.L., and C.S.W.L. designed the experiments. A.H.K.F. and Y.H. performed experiments and analyzed the data. A.H.K.F. and B.W.L.S. performed plasmid constructs cloning and *in utero* electroporation experiments. Q.Z. and C.C.S.T. wrote code for data analysis. A.H.K.F., Y.H., and X.L. performed awake animal imaging. K.K.-Y.W., J.H., K.-O.L., and C.S.W.L. supervised experiments and provided resources. A.H.K.F., Y.H., K.-O.L., and C.S.W.L. wrote and edited the manuscript with comments from all the other authors.

DECLARATION OF INTERESTS

The authors declare no competing interests.

Received: April 19, 2023
Revised: December 21, 2023
Accepted: February 16, 2024
Published: March 7, 2024

REFERENCES

1. Hirokawa, N., Noda, Y., Tanaka, Y., and Niwa, S. (2009). Kinesin superfamily motor proteins and intracellular transport. Nat. Rev. Mol. Cell Biol. *10*, 682–696. https://doi.org/10.1038/nrm2774.
2. Dictenberg, J.B., Swanger, S.A., Antar, L.N., Singer, R.H., and Bassell, G.J. (2008). A direct role for FMRP in activity-dependent dendritic mRNA transport links filopodial-spine morphogenesis to fragile X

syndrome. Dev. Cell *14*, 926–939. https://doi.org/10.1016/j.devcel.2008.04.003.

3. Yoo, K.-S., Lee, K., Oh, J.-Y., Lee, H., Park, H., Park, Y.S., and Kim, H.K. (2019). Postsynaptic density protein 95 (PSD-95) is transported by KIF5 to dendritic regions. Mol. Brain *12*. 97–12.
4. Pan, F., Aldridge, G.M., Greenough, W.T., and Gan, W.-B. (2010). Dendritic spine instability and insensitivity to modulation by sensory experience in a mouse model of fragile X syndrome. Proc. Natl. Acad. Sci. USA *107*, 17768–17773.
5. Subramanian, J., Michel, K., Benoit, M., and Nedivi, E. (2019). CPG15/Neuritin Mimics Experience in Selecting Excitatory Synapses for Stabilization by Facilitating PSD95 Recruitment. Cell Rep. *28*, 1584–1595.e5.
6. Nimchinsky, E.A., Oberlander, A.M., and Svoboda, K. (2001). Abnormal development of dendritic spines in FMR1 knock-out mice. J. Neurosci. *21*, 5139–5146. https://doi.org/10.1523/JNEUROSCI.21-14-05139.2001.
7. Khayachi, A., Gwizdek, C., Poupon, G., Alcor, D., Chafai, M., Cassé, F., Maurin, T., Prieto, M., Folci, A., De Graeve, F., et al. (2018). Sumoylation regulates FMRP-mediated dendritic spine elimination and maturation. Nat. Commun. *9*, 757.
8. Maas, C., Belgardt, D., Lee, H.K., Heisler, F.F., Lappe-Siefke, C., Magiera, M.M., van Dijk, J., Hausrat, T.J., Janke, C., and Kneussel, M. (2009). Synaptic activation modifies microtubules underlying transport of postsynaptic cargo. Proc. Natl. Acad. Sci. USA *106*, 8731–8736.
9. Kanai, Y., Okada, Y., Tanaka, Y., Harada, A., Terada, S., and Hirokawa, N. (2000). KIF5C, a novel neuronal kinesin enriched in motor neurons. J. Neurosci. *20*, 6374–6384.
10. Zhao, J., Fok, A.H.K., Fan, R., Kwan, P.-Y., Chan, H.-L., Lo, L.H.-Y., Chan, Y.-S., Yung, W.-H., Huang, J., Lai, C.S.W., and Lai, K.O. (2020). Specific depletion of the motor protein KIF5B leads to deficits in dendritic transport, synaptic plasticity and memory. Elife *9*, e53456.
11. Cromberg, L.E., Saez, T.M.M., Otero, M.G., Tomasella, E., Alloatti, M., Damianich, A., Pozo Devoto, V., Ferrario, J., Gelman, D., Rubinstein, M., and Falzone, T.L. (2019). Neuronal KIF5b deletion induces striatum-dependent locomotor impairments and defects in membrane presentation of dopamine D2 receptors. J. Neurochem. *149*, 362–380. https://doi.org/10.1111/jnc.14665.
12. Lai, C.S.W., Franke, T.F., and Gan, W.B. (2012). Opposite effects of fear conditioning and extinction on dendritic spine remodelling. Nature *483*, 87–91. https://doi.org/10.1038/nature10792.
13. Zhou, Y., Lai, C.S.W., Bai, Y., Li, W., Zhao, R., Yang, G., Frank, M.G., and Gan, W.-B. (2020). REM sleep promotes experience-dependent dendritic spine elimination in the mouse cortex. Nat. Commun. *11*, 4819.
14. Opris, I., Hampson, R.E., Stanford, T.R., Gerhardt, G.A., and Deadwyler, S.A. (2011). Neural activity in frontal cortical cell layers: evidence for columnar sensorimotor processing. J. Cogn. Neurosci. *23*, 1507–1521.
15. DeNardo, L.A., Berns, D.S., DeLoach, K., and Luo, L. (2015). Connectivity of mouse somatosensory and prefrontal cortex examined with trans-synaptic tracing. Nat. Neurosci. *18*, 1687–1697.
16. Villa, K.L., Berry, K.P., Subramanian, J., Cha, J.W., Oh, W.C., Kwon, H.-B., Kubota, Y., So, P.T.C., and Nedivi, E. (2016). Inhibitory synapses are repeatedly assembled and removed at persistent sites in vivo. Neuron *89*, 756–769.
17. Chen, J.L., Villa, K.L., Cha, J.W., So, P.T.C., Kubota, Y., and Nedivi, E. (2012). Clustered dynamics of inhibitory synapses and dendritic spines in the adult neocortex. Neuron *74*, 361–373. https://doi.org/10.1016/j.neuron.2012.02.030.
18. Isshiki, M., Tanaka, S., Kuriu, T., Tabuchi, K., Takumi, T., and Okabe, S. (2014). Enhanced synapse remodelling as a common phenotype in mouse models of autism. Nat. Commun. *5*, 4742. https://doi.org/10.1038/ncomms5742.
19. Boivin, J.R., and Nedivi, E. (2018). Functional implications of inhibitory synapse placement on signal processing in pyramidal neuron dendrites. Curr. Opin. Neurobiol. *51*, 16–22.
20. Cane, M., Maco, B., Knott, G., and Holtmaat, A. (2014). The relationship between PSD-95 clustering and spine stability in vivo. J. Neurosci. *34*, 2075–2086.
21. Antar, L.N., and Bassell, G.J. (2003). Sunrise at the synapse: the FMRP mRNP shaping the synaptic interface. Neuron *37*, 555–558. https://doi.org/10.1016/s0896-6273(03)00090-4.
22. Westmark, C.J. (2013). FMRP: a triple threat to PSD-95. Front. Cell. Neurosci. *7*, 57. https://doi.org/10.3389/fncel.2013.00057.
23. Tsai, N.P., Wilkerson, J.R., Guo, W., Maksimova, M.A., DeMartino, G.N., Cowan, C.W., and Huber, K.M. (2012). Multiple autism-linked genes mediate synapse elimination via proteasomal degradation of a synaptic scaffold PSD-95. Cell *151*, 1581–1594. https://doi.org/10.1016/j.cell.2012.11.040.
24. Todd, P.K., Mack, K.J., and Malter, J.S. (2003). The fragile X mental retardation protein is required for type-I metabotropic glutamate receptor-dependent translation of PSD-95. P Natl Acad Sci USA *100*, 14374–14378. https://doi.org/10.1073/pnas.2336265100.
25. Muddashetty, R.S., Nalavadi, V.C., Gross, C., Yao, X., Xing, L., Laur, O., Warren, S.T., and Bassell, G.J. (2011). Reversible inhibition of PSD-95 mRNA translation by miR-125a, FMRP phosphorylation, and mGluR signaling. Mol. Cell *42*, 673–688. https://doi.org/10.1016/j.molcel.2011.05.006.
26. Kanai, Y., Dohmae, N., and Hirokawa, N. (2004). Kinesin transports RNA: isolation and characterization of an RNA-transporting granule. Neuron *43*, 513–525. https://doi.org/10.1016/j.neuron.2004.07.022.
27. Feng, Y., Gutekunst, C.A., Eberhart, D.E., Yi, H., Warren, S.T., and Hersch, S.M. (1997). Fragile X mental retardation protein: nucleocytoplasmic shuttling and association with somatodendritic ribosomes. J. Neurosci. *17*, 1539–1547, 1997. https://doi.org/10.1523/JNEUROSCI.17-05-01539.
28. Ferrari, F., Mercaldo, V., Piccoli, G., Sala, C., Cannata, S., Achsel, T., and Bagni, C. (2007). The fragile X mental retardation protein-RNP granules show an mGluR-dependent localization in the post-synaptic spines. Mol. Cell. Neurosci. *34*, 343–354. https://doi.org/10.1016/j.mcn.2006.11.015.
29. Kao, D.I., Aldridge, G.M., Weiler, I.J., and Greenough, W.T. (2010). Altered mRNA transport, docking, and protein translation in neurons lacking fragile X mental retardation protein. Proc. Natl. Acad. Sci. USA *107*, 15601–15606. https://doi.org/10.1073/pnas.1010564107.
30. Weiler, I.J., Irwin, S.A., Klintsova, A.Y., Spencer, C.M., Brazelton, A.D., Miyashiro, K., Comery, T.A., Patel, B., Eberwine, J., and Greenough, W.T. (1997). Fragile X mental retardation protein is translated near synapses in response to neurotransmitter activation. Proc. Natl. Acad. Sci. USA *94*, 5395–5400. https://doi.org/10.1073/pnas.94.10.5395.
31. Antar, L.N., Afroz, R., Dictenberg, J.B., Carroll, R.C., and Bassell, G.J. (2004). Metabotropic glutamate receptor activation regulates fragile x mental retardation protein and FMR1 mRNA localization differentially in dendrites and at synapses. J. Neurosci. *24*, 2648–2655. https://doi.org/10.1523/JNEUROSCI.0099-04.2004.
32. Antar, L.N., Dictenberg, J.B., Plociniak, M., Afroz, R., and Bassell, G.J. (2005). Localization of FMRP-associated mRNA granules and requirement of microtubules for activity-dependent trafficking in hippocampal neurons. Genes Brain Behav. *4*, 350–359. https://doi.org/10.1111/j.1601-183X.2005.00128.x.
33. Sidorov, M.S., Auerbach, B.D., and Bear, M.F. (2013). Fragile X mental retardation protein and synaptic plasticity. Mol. Brain *6*, 15. https://doi.org/10.1186/1756-6606-6-15.
34. Cruz-Martín, A., Crespo, M., and Portera-Cailliau, C. (2010). Delayed stabilization of dendritic spines in fragile X mice. J. Neurosci. *30*, 7793–7803. https://doi.org/10.1523/JNEUROSCI.0577-10.2010.
35. Jiang, M., Ash, R.T., Baker, S.A., Suter, B., Ferguson, A., Park, J., Rudy, J., Torsky, S.P., Chao, H.T., Zoghbi, H.Y., and Smirnakis, S.M. (2013). Dendritic arborization and spine dynamics are abnormal in the mouse model

of MECP2 duplication syndrome. J. Neurosci. *33*, 19518–19533. https://doi.org/10.1523/JNEUROSCI.1745-13.2013.

36. Fénelon, K., Xu, B., Lai, C.S., Mukai, J., Markx, S., Stark, K.L., Hsu, P.K., Gan, W.B., Fischbach, G.D., MacDermott, A.B., et al. (2013). The pattern of cortical dysfunction in a mouse model of a schizophrenia-related microdeletion. J. Neurosci. *33*, 14825–14839. https://doi.org/10.1523/JNEUROSCI.1611-13.2013.
37. Huang, Y., Jiang, H., Zheng, Q., Fok, A.H.K., Li, X., Lau, C.G., and Lai, C.S.W. (2021). Environmental enrichment or selective activation of parvalbumin-expressing interneurons ameliorates synaptic and behavioral deficits in animal models with schizophrenia-like behaviors during adolescence. Mol. Psychiatry *26*, 2533–2552. https://doi.org/10.1038/s41380-020-01005-w.
38. Burgin, K.E., Waxham, M.N., Rickling, S., Westgate, S.A., Mobley, W.C., and Kelly, P.T. (1990). In situ hybridization histochemistry of Ca2+/calmodulin-dependent protein kinase in developing rat brain. J. Neurosci. *10*, 1788–1798. https://doi.org/10.1523/JNEUROSCI.10-06-01788.1990.
39. Dragatsis, I., and Zeitlin, S. (2000). CaMKIIalpha-Cre transgene expression and recombination patterns in the mouse brain. Genesis *26*, 133–135.
40. Tsien, J.Z., Chen, D.F., Gerber, D., Tom, C., Mercer, E.H., Anderson, D.J., Mayford, M., Kandel, E.R., and Tonegawa, S. (1996). Subregion- and cell type-restricted gene knockout in mouse brain. Cell *87*, 1317–1326. https://doi.org/10.1016/s0092-8674(00)81826-7.
41. Cui, J., Wang, Z., Cheng, Q., Lin, R., Zhang, X.M., Leung, P.S., Copeland, N.G., Jenkins, N.A., Yao, K.M., and Huang, J.D. (2011). Targeted inactivation of kinesin-1 in pancreatic beta-cells in vivo leads to insulin secretory deficiency. Diabetes *60*, 320–330. https://doi.org/10.2337/db09-1078.
42. Maas, C., Tagnaouti, N., Loebrich, S., Behrend, B., Lappe-Siefke, C., and Kneussel, M. (2006). Neuronal cotransport of glycine receptor and the scaffold protein gephyrin. J. Cell Biol. *172*, 441–451.
43. Tsuriel, S., Geva, R., Zamorano, P., Dresbach, T., Boeckers, T., Gundelfinger, E.D., Garner, C.C., and Ziv, N.E. (2006). Local sharing as a predominant determinant of synaptic matrix molecular dynamics. PLoS Biol. *4*, e271.
44. Bresler, T., Ramati, Y., Zamorano, P.L., Zhai, R., Garner, C.C., and Ziv, N.E. (2001). The dynamics of SAP90/PSD-95 recruitment to new synaptic junctions. Mol. Cell. Neurosci. *18*, 149–167.
45. Gray, N.W., Weimer, R.M., Bureau, I., and Svoboda, K. (2006). Rapid redistribution of synaptic PSD-95 in the neocortex in vivo. PLoS Biol. *4*, e370.
46. Hu, X., Ballo, L., Pietila, L., Viesselmann, C., Ballweg, J., Lumbard, D., Stevenson, M., Merriam, E., and Dent, E.W. (2011). BDNF-induced increase of PSD-95 in dendritic spines requires dynamic microtubule invasions. J. Neurosci. *31*, 15597–15603.
47. Richter, J.D., and Zhao, X. (2021). The molecular biology of FMRP: new insights into fragile X syndrome. Nat. Rev. Neurosci. *22*, 209–222. https://doi.org/10.1038/s41583-021-00432-0.
48. De Diego Otero, Y., Severijnen, L.A., van Cappellen, G., Schrier, M., Oostra, B., and Willemsen, R. (2002). Transport of fragile X mental retardation protein via granules in neurites of PC12 cells. Mol. Cell Biol. *22*, 8332–8341. https://doi.org/10.1128/MCB.22.23.8332-8341.2002.
49. El Fatimy, R., Davidovic, L., Tremblay, S., Jaglin, X., Dury, A., Robert, C., De Koninck, P., and Khandjian, E.W. (2016). Tracking the Fragile X Mental Retardation Protein in a Highly Ordered Neuronal RiboNucleoParticles Population: A Link between Stalled Polyribosomes and RNA Granules. PLoS Genet. *12*, e1006192. https://doi.org/10.1371/journal.pgen.1006192.
50. Mikuni, T., Nishiyama, J., Sun, Y., Kamasawa, N., and Yasuda, R. (2016). High-throughput, high-resolution mapping of protein localization in mammalian brain by in vivo genome editing. Cell *165*, 1803–1817.
51. Matsuda, T., and Cepko, C.L. (2007). Controlled expression of transgenes introduced by in vivo electroporation. Proc. Natl. Acad. Sci. USA *104*, 1027–1032. https://doi.org/10.1073/pnas.0610155104.
52. Ascano, M., Jr., Mukherjee, N., Bandaru, P., Miller, J.B., Nusbaum, J.D., Corcoran, D.L., Langlois, C., Munschauer, M., Dewell, S., Hafner, M., et al. (2012). FMRP targets distinct mRNA sequence elements to regulate protein expression. Nature *492*, 382–386. https://doi.org/10.1038/nature11737.
53. Schneider, C.A., Rasband, W.S., and Eliceiri, K.W. (2012). NIH Image to ImageJ: 25 years of image analysis. Nat. Methods *9*, 671–675. https://doi.org/10.1038/nmeth.2089.
54. Cui, J., Wang, Z., Cheng, Q., Lin, R., Zhang, X.-M., Leung, P.S., Copeland, N.G., Jenkins, N.A., Yao, K.-M., and Huang, J.-D. (2011). Targeted inactivation of kinesin-1 in pancreatic β-cells in vivo leads to insulin secretory deficiency. Diabetes *60*, 320–330.
55. Ng, L.H.L., Huang, Y., Han, L., Chang, R.C.-C., Chan, Y.S., and Lai, C.S.W. (2018). Ketamine and selective activation of parvalbumin interneurons inhibit stress-induced dendritic spine elimination. Transl. Psychiatry *8*, 272.

STAR★METHODS

KEY RESOURCES TABLE

REAGENT or RESOURCE	SOURCE	IDENTIFIER
Chemicals, peptides, and recombinant proteins		
Buprenorphine (Temgesic®)	Indivior	Reg no: HK-28719
Carprofen (Rimadyl®)	Zoetis UK	N/A
Dexamethasone	Sigma-Aldrich	CAS: 2392-39-4
Enrofloxacin (Baytril®)	Bayer AG	N/A
Ketamine/Xylazine	Alfasan International B.V.	Reg no: HK-37715/HK-56179
Isoflurane	RWD Life Science	Cat#R510-22-16
Experimental models: Organisms/strains		
Mouse: B6.Cg-Tg(CaMK2α-cre) T29-1Stl/J	The Jackson Laboratory	JAX#005359
Mouse: B6.Cg-Gt(ROSA)26Sortm9(CAG-tdTomato)Hze/J	The Jackson Laboratory	JAX#007909
Mouse: Kif5b$^{fl/fl}$ mice	Cui et al.[41]	N/A
Oligonucleotides		
Genotyping primers for Kif5b$^{fl/fl}$ mice	Cui et al.[41]	N/A
Primers: FMRP forward: 5′- gttgcaaccggttccggactcagatctcgagc -3’; FMRP reverse: 5′- gttgcagcggccgcttagggtactccattcacg -3′	This paper	N/A
Primers: GFP forward: 5′- cggccagaattctgatggtgagcaagggcgagg-3’; GFP reverse: 5′- cggccaaccggtcttgtacagctcgtccatgc-3′	This paper	N/A
Recombinant DNA		
pAAV-CAG-GFP	Edward Boyden	Addgene#37825
pCAG-Cre	Matsuda et al.[51]	Addgene#13775
pCALNL-DsRed	Matsuda et al.[51]	Addgene#13769
pFU-dio-YFP-W	Villa et al.[16]	Addgene#73858
pFU-dio-PSD95-mCherry	Villa et al.[16]	Addgene#73919
pFU-dio-Teal-gephyrin-W	Villa et al.[16]	Addgene#73918
pFRT-TODestFLAGHAhFMRPiso1	Ascano et al.[52]	Addgene#48690
pCALNL-GFP	This paper, subcloning	N/A
pCALNL-GFP-FMRP	This paper, subcloning	N/A
pCAG-DsRed	Isshiki et al.[18]	N/A
Software and algorithms		
Fiji	Schneider et al.[53]	SCR_002285
Metamorph	Molecular devices	SCR_002368
Imaris	Bitplane Imaris	SCR_007370
MATLAB	MathWorks	SCR_001622
GraphPad Prism	GraphPad Software	SCR_002798
MATLAB code for analysis	Deposited at GitHub	Zenodo: https://doi.org/10.5281/zenodo.10571308

RESOURCE AVAILABILITY

Lead contact

Further information and requests for resources and reagents should be directed to and will be fulfilled by the lead contact, Dr. Cora S.W. Lai (coraswl@hku.hk).

Materials availability

Further information and requests for mouse reagent should be directed to and will be fulfilled by Dr. Cora S.W. Lai (coraswl@hku.hk).

Data and code availability

- The data supporting the findings of this study will be shared by the lead contact upon request.
- The MATLAB code has been deposited at GitHub and is publicly available as of the date of publication. DOI is listed in the key resources table.
- Any additional information required to re-analyze the data reported in this paper will be provided by the lead contact upon request.

EXPERIMENTAL MODEL AND STUDY PARTICIPANT DETAILS

Animals

CaMKIIα-Cre (JAX#005359) and Ai9 (JAX# 007909) mice were purchased from the Jackson Laboratory. *Kif5b*$^{fl/fl}$ mice were gifts from Prof. Jiang-Dong Huang's lab.[54] *CaMKIIα*-Cre knock-in mice were used to breed with mice homozygous for the *Kif5b*$^{fl/fl}$ transgene to yield KIF5B cKO (*CaMKIIα*-Cre; *Kif5b*$^{fl/fl}$) mice. *CaMKIIα*-Cre mice were used as control. Both males and females were used in this study by random sampling. Mice were group-housed under a 12 h light/dark cycle in the Center for Comparative Medicine Research, The University of Hong Kong, accredited by Association for Assessment and Accreditation of Laboratory Animal Care International. Food and water were provided *ad libitum*. 4–5 weeks old mice were used in this study. All experiments were approved and performed in accordance with the University of Hong Kong Committee on the Use of Live Animals in Teaching and Research guidelines.

METHOD DETAILS

Auditory-cued fear conditioning and fear extinction

FreezeFrame system (Coulbourn Instruments) was used to train and test mice. Each fear conditioning chamber was contained in a sound-attenuating enclosure (Coulbourn Instruments). Actimetrics FreezeFrame software (version 2.2; Coulbourn Instruments) was used to control the stimulus presentation by a pre-set program. For training, the fear conditioning chamber was equipped with stainless-steel shocking grids, which connected to a precision feedback current-regulated shocker (Coulbourn Instruments). Mice were habituated for 1 min on a shocking grid (context A: shocking floor grids, ethanol scent). Fear conditioning was conducted by presenting a 30 s, 4000 Hz, 80 dB auditory cue (CS) and then with a 2 s, 0.5 mA scrambled foot shock (US) at the end of tone presentation. The intertrial interval was 20 s. One min after conditioning, mice were returned to their home cages. For recall testing, the shocking grids were replaced with non-shocking test grids that was different from the shocking grids used during conditioning. Mice were placed in a different context (context B: patterned chamber walls, test floor grids, 1% Pinesol) for an initial 2-min period (pre-CS) and this was followed by tone presentation for 2 min (CS). Each trial of fear extinction was the same as the setting of the recall test. Fear extinction was carried out in two days with 5 trials per day. Animals were recorded using low-light video cameras throughout the test. All equipment was thoroughly cleaned with water.

DNA constructs

pAAV-CAG-GFP, pCAG-Cre, pCALNL-DsRed, pFU-dio-YFP-W, pFU-dio-PSD95-mCherry and pFU-dio-Teal-gephyrin-W were purchased from Addgene. pCAG-DsRed was a gift from Prof. Shigeo Okabe.[18] pCALNL-GFP-FMRP was constructed by amplifying the *FMR1* gene from the plasmid, pFRT-TODestFLAGHAhFMRPiso1, which was purchased from Addgene, with forward primer: 5′-gttgcaaccggttccggactcagatctcgagc -3′ and reverse primer: 5′- gttgcagcggccgcttagggtactccattcacg -3'. *EGFP* gene was amplified from pEGFP-C1, purchased from Addgene, with forward primer: 5′-cggccagaattctgatggtgagcaagggcgagg-3′ and reverse primer: 5′-cggccaaccggtcttgtacagctcgtccatgc-3'. The *FMR1* insert was subcloned into AgeI and NotI cloning sites of pCALNL-DsRed. *EGFP* insert was subcloned into EcoRI and AgeI cloning sites of the vector pCALNL-DsRed. The original dsRed insert of the vector plasmid would be removed during the digestion step as a result. The resulting plasmid was a Cre recombinase-dependent expression plasmid of the insert GFP-FMRP.

In utero electroporation

In utero electroporation was carried out on mouse embryos of embryonic day (E) 14.5–15.5 to target progenitors that are destined to layer 2/3. Pregnant mice were anesthetized by subcutaneously injecting ketamine/xylazine (20 mg/mL and 3 mg/mL, respectively in saline, 6 μL/g body weight). A 3 mm incision was made at the abdomen to expose the uterine horns. Around 1 μL of plasmid solution was microinjected into the right brain ventricle of the embryos. A pair of tweezer-type electrodes was placed on the embryonic brains with the positive electrode contacting the frontal cortex. Five 50 ms square electric pulses at 1 Hz were applied with an electroporator (BTX, Harvard Bioscience, Inc). The voltage used depends on the plasmids mix in the injecting solution. For experiments in Figures 1 and 2 (pCAG-Cre, pFU-dio-YFP-W, pFU-dio-PSD95-mCherry and pFU-dio-Teal-gephyrin-W) and Figures 3 and 4 (pCAG-Cre, pCALNL-DsRed and pCALNL-GFP-FMRP), 30–35 V was used. For experiments in Figure S2B (pCAG-Cre, pCALNL-GFP, pcDNA3.1) and Figures S2C–S2H (pCAG-Cre, pFU-dio-YFP-W), 25–35 V was used. After electroporation, embryos were gently placed back into the abdomen and the incision was sutured.

In vivo imaging of dendritic spines, synaptic markers and FMRP-GFP

Preparation for thinned-skull window imaging

Dendritic spine plasticity in Figure S2 (Figure S2C–S2H) was examined in longitudinal experiment by imaging the mouse cortex through a thinned-skull window as described previously.[12] One-month-old mice were anesthetized with ketamine/xylazine injection (intraperitoneally, 20 mg/mL, 3 mg/mL respectively in saline, 6 μL/g body weight) and head-fixed to an imaging platform by cyanoacrylate glue. Thinned-skull windows were made with high-speed microdrills. Skull thickness was reduced to about 20 μm. Artificial cerebrospinal fluid (ACSF) was used to moist the drilling area to reduce friction-induced temperature rise. ACSF contained 119mM NaCl, 2.5 mM $CaCl_2$, 1 mM NaH_2PO_4, 2.5 mM KCl, 1.3 mM $MgSO_4$, 26.2 mM $NaHCO_3$, and 22 mM glucose. A two-photon microscope (25X water immersion lens, N.A. = 1.05) was used to acquire images. For re-imaging, previous regions were identified by aligning the brain vasculature. Microsurgical blades would be required to re-thin the region of interest. The area of the imaging region was 216 μm × 216 μm. The center of imaging region was located at the frontal association cortex (+2.8 mm bregma, +1.0 mm midline).

Preparation of cranial window

Cranial window implantation protocol was as described previously.[37,55] P27 ± 2 mice were anesthetized by intraperitoneal injection of ketamine/xylazine (20 mg/mL, 3 mg/mL respectively in saline, 6 μL/g body weight). Three drugs were given prophylactically including dexamethasone (2 mg/kg, Sigma-Aldrich), carprofen (5 mg/kg, Norbrook Laboratories Ltd) and buprenorphine (0.1 mg/kg, Indivior Pty Ltd) to lower intracranial pressure, reduce surgery-induced inflammation and relief pain, respectively. Scalp was removed and a customized metallic head-mount was glued to the skull by cyanoacrylate glue and dental acrylic cement (Megadental GmbH) for the purpose of fixing mouse heads onto surgical and future imaging platforms. A craniotomy (square area about 2 mm × 2 mm) was made and replaced by a #2 glass coverslip (Thermo Fisher Scientific) of the same size. The seams between the coverslip and the skull were sealed by firstly a layer of tissue adhesive (Vetbond, 3M Company) and secondly a layer of cyanoacrylate glue. Finally, dental acrylic cement was applied to cover the exposed skull and to secure the metallic head-mount. As post-operative prescription, mice were given carprofen (5 mg/kg) and buprenorphine (0.1 mg/kg) twice a day for 5 days. Enrofloxacin (Baytril, 2.5% oral solution) was administered in drinking water (diluted to 0.5%) to prevent microbial infection. Mice will be recovered for 10-day before imaging.

Two-photon imaging

Mice were anesthetized by ketamine/xylazine and head-fixed onto a customized platform. The two-photon microscope (Olympus FVMPE-RS) used was equipped with two lasers with tuning range from 680 nm to 1080 nm (Chameleon Vision II, Coherent). To image YFP signal, GFP signal or Teal (mTFP1) signal, a laser of 880 nm was used. To image dsRed signal or mCherry signal, a laser of 1080 nm was used. Independent filters were used for three different channels (Blue: 435–485 nm, Green/Yellow: 510–560 nm, Red: LP590 nm). The water immersion objective lens had a magnification of 25× and a numerical aperture (N.A.) of 1.05. z stack images of dendritic spines, synaptic markers, and FMRP puncta were acquired at high resolution (0.14 μm/pixel XY resolution, 0.75 μm step size). The maximum area of imaging field was 216 × 216 μm. The region of interest was at the frontal association cortex (+2.8 mm bregma, +1.0 mm midline).

Awake imaging

For head-fixed awake imaging, an air-suspended platform (Mobile HomeCage, Neurotar) was used, which comprised of a lightweight carbon fiber cage and an air-cushion generating system. Mice used for awake imaging were implanted with a customized metallic head-mount that provided a tight-fit to the head-fix clamping system of Mobile HomeCage. Mice with head mount were clamped on the platform and placed into air-lifted carbon fiber cage so that mice could move freely with head-fixation. The air cushion also provided shock-absorbance effect to stabilize the head-fixing and image acquisition. The whole platform with the head-fixed mouse was placed under the 2-photon microscope objective lens for image acquisition. At the end of an imaging session, mice were released from platform and returned to home cage.

QUANTIFICATION AND STATISTICAL ANALYSIS

Data analysis

Analysis for dendritic spines

Metamorph software (Molecular Devices) was used to analyze dendritic spine plasticity from 3D-image stacks. The criteria of identifying dendritic protrusions were as described previously.[37,55] Briefly, the number and location of dendritic protrusions, which protrusion lengths were more than one-third of the dendritic shaft diameter, were tracked manually along with the dendritic segments. Dendritic protrusions were classified into filopodia and spines. Filopodia were identified as long, thin structures (generally larger than twice the average spine length, the ratio of head diameter to neck diameter <1.2:1, and ratio of length to neck diameter >3:1). The remaining protrusions were classified as spines. Spines were considered as identical between views if their positions were unchanged with respect to adjacent landmarks. Dendritic segments were randomly sampled within the stacks of images acquired, which covered a maximum volume of 216 μm × 216 μm × 100 μm below the pia surface. Images were processed by 2D-deconvolution in Metamorph software. Dendritic spine plasticity was tracked across different time points. Three-dimensional stacks were used for analysis instead of z-projection images to ensure that tissue movements and rotation between imaging intervals did not hinder spine identification. Spines were identified as stable between time points if their positions remained the same with regards to adjacent landmarks. The percentage of spines/puncta formation and elimination represented the number of spines/puncta formed or eliminated between the first and second view divided by the total number of spines/puncta counted at the first view in each mouse.

Unless specified, the n number for analysis of imaging experiments refers to the number of animals analyzed in each group. For image display, images of dendrites were highlighted by removing irrelevant dendrites and out-of-focus dendritic spines manually using Adobe Photoshop. The resulting image stacks that highlight the dendrites of interest were then projected to generate two-dimensional images and adjusted for contrast and brightness.

Scoring for synaptic markers and FMRP-GFP puncta

Metamorph software (Molecular Devices) were used to analyze the dynamics and localization of synaptic marker and FMRP-GFP puncta. Similar to the analysis method of dendritic spines, images were first processed by 2D-deconvolution. The identification of synaptic marker puncta or FMRP puncta was defined by the following 3 criteria: (1) The signal was clustered over at least 6 pixels; (2) The signal was present in at least two contiguous z planes; (3) The signal intensity was higher than 3 times of the background noise. The presence and absence of synaptic markers or FMRP-GFP puncta at each time point were counted and calculated.

Measurement of FMRP localization

Every dendrite was assumed to be a 1-D linear structure for this analysis. Every dendritic spine and FMRP puncta could then be registered with a location datum, which was the distance away from the reference spine measured with Metamorph software (Molecular Devices). And the location datum for the reference spine was set to be zero. Custom-written MATLAB codes were used to calculate and tabulate all possible distance measurements between the locations of FMRP puncta and all dendritic spines. Therefore, the closest relative distance between dendritic spine and FMRP punctum were identified and plotted into a box-and-whisker diagram.

FMRP distribution simulation

In order to determine if FMRP puncta are distributed randomly along individual dendritic segments, we calculated the distance between the location of closest FMRP puncta pair, or between the location of closest FMRP puncta and dendritic spine pair. We used custom-written MATLAB codes to simulate the location of FMRP puncta along the dendritic segments. The simulation was conducted under the assumption that the FMRP puncta are distributed randomly (uniform statistical distribution) along dendritic segments. Accordingly, we generated FMRP puncta at random positions along dendritic segments, considering the actual lengths of dendrites and the numbers of FMRP puncta observed in the data. Subsequently, we calculated the closest distance between the simulated FMRP puncta pair or between the actual location of dendritic spine and the simulated FMRP puncta. We then repeated this simulation 1,000 times to generate the null distribution of closest distances along dendritic segments under the assumption of FMRP puncta random distribution. Finally, we compared the cumulative probabilities of distances calculated from the observed data and from the simulation using Kolmogorov-Smirnov test.

Measurement of dendritic length

Each dendrite analyzed was measured with either Imaris or the ImageJ plugin, SNT. The software measures accurate distance of a dendrite by reconstruction of path considering the 3D reconstruction of the z stack images. Total dendritic length analyzed was thus obtained by summing up all the individual dendritic lengths in each sample group. The average length ±SD per mouse is also presented in the respective figure legends.

Total dendritic length and dendritic spine counts

Figure 1: Control: n = 6 mice, total 1112 dendritic spines, in which Dual +ve 433 spines, PSD95-only 323 spines, gephyrin-only (Gep-only) 104 spines, Dual -ve 252 spines, on Day 0. KIF5B cKO: n = 7 mice, total 1020 dendritic spines, in which Dual +ve 295 spines, PSD95-only 253 spines, Gep-only 67 spines, Dual -ve 405 spines, on Day 0. Total analyzed dendrite lengths are 1721.2 μm (Control) and 1347.1 μm (KIF5B cKO). Average dendritic length analyzed (±SD) is 286.9 ± 56.2 μm (Control) and 192.4 ± 63.8 μm (KIF5B cKO).

Figure 2: Control: n = 6 mice, total 1112 dendritic spines, 756 PSD95-positive spines, 356 PSD95-negative spines, 537 Gep-positive spines, 575 Gep-negative spines, on Day 0. KIF5B cKO: n = 7 mice, total 1020 dendritic spines, 550 PSD95-positive spines, 470 PSD95-negative spines, 362 Gep-positive spines, 658 Gep-negative spines, on Day 0. Total analyzed dendrite lengths are 1721.2 μm (Control) and 1347.1 μm (KIF5B cKO). Average dendritic length analyzed (±SD) is 286.9 ± 56.2 μm (Control) and 192.4 ± 63.8 μm (KIF5B cKO).

Figure 3: Control: n = 6 mice, total 1138 dendritic spines and 393 FMRP puncta, at H0; KIF5B cKO: n = 5 mice, total 740 dendritic spines and 305 FMRP puncta, at H0. Total analyzed dendrite lengths are 2241.24 μm (Control) and 1905.96 μm (KIF5B cKO). Average dendritic length analyzed (±SD) is 373.5 ± 47.7 μm (Control) and 382.0 ± 97.5 μm (KIF5B cKO).

Figure 4: Control unpaired: n = 6 mice, total 1088 dendritic spines and 377 FMRP puncta; Control paired: n = 4 mice, total 698 dendritic spines and 144 FMRP puncta; KIF5B cKO paired: n = 4 mice, total 708 dendritic spines and 244 FMRP puncta. Total analyzed dendrite lengths are 2305.67 μm (Control unpaired), 1989.08 μm (Control paired) and 1787.63 μm (KIF5B cKO paired). Average dendritic length analyzed (±SD) is 398.9 ± 51.4 μm (Control unpaired), 497.3 ± 135.8 μm (Control paired) and 446.9 ± 59.1 μm (KIF5B cKO paired).

Statistical analysis

For statistical analysis, GraphPad Prism software version 8.0 (GraphPad Software) was used. Each data point in graphical representation indicates one mouse unless otherwise specified. To test for normal distribution of data, Shapiro-Wilk test was used. Q-Q plot was used to confirm normality in two-way ANOVA test. For normally distributed data, either one-way ANOVA or Student's *t*-test was used to compare means between multiple groups or two groups, respectively. For non-normally distributed data, either Mann-Whitney *U*-test or Kruskal-Wallis test was used for 2-group comparisons or multiple-group comparisons, respectively. For comparison of data with 2 independent variables, two-way ANOVA was used instead of one-way ANOVA. *Post hoc* tests were carried out

when significantly different results (p values less than 0.05) were found. Tukey's test was used for both one-way ANOVA and two-way ANOVA. Sidak multiple comparison test was used for two-way ANOVA when the number of groups to be compared was only two. Dunn's test was used for Kruskal-Wallis test. Kruskal-Wallis test was also used as a statistical test for the median for the analysis of FMRP localization. *Post hoc* Dunn's test was used for the multiple comparison. Pearson's correlation coefficient analysis was used for the simple linear regression. Kolmogorov-Smirnov test was used to compare cumulative distribution fractions. In all analyses, p values less than 0.05 were considered as statistically significant.